M 2015

U.PORTO
FEUP FACULDADE DE ENGENHARIA
UNIVERSIDADE DO PORTO

FUNCTIONALIZED GOLD NANOPARTICLES AS ANTICANCER DRUG DELIVERY SYSTEMS

DANIEL PEDRO PIRES ALVES REIS

DISSERTAÇÃO DE MESTRADO APRESENTADA
À FACULDADE DE ENGENHARIA DA UNIVERSIDADE DO PORTO EM
ENGENHARIA BIOMÉDICA

U.PORTO

FEUP FACULDADE DE ENGENHARIA UNIVERSIDADE DO PORTO

MEB - MESTRADO EM ENGENHARIA BIOMÉDICA | **2014/2015**

A Dissertação intitulada

"Functionalized Gold Nanoparticles as Anticancer Drug Delivery Systems"

foi aprovada em provas realizadas em 21-10-2015

o júri

Presidente Professor Doutor Jorge Alves da Silva
Professor Auxiliar do Departamento de Engenharia Informática da Faculdade de Engenharia da U. Porto

Doutor Bruno Filipe Carmelino Cardoso Sarmento
Investigador do Instituto de Engenharia Biomédica da U. Porto

Professor Doutor Manuel Álvaro Neto Coelho
Professor Auxiliar do Departamento de Engenharia Química da Faculdade de Engenharia da U. Porto

O autor declara que a presente dissertação (ou relatório de projeto) é da sua exclusiva autoria e foi escrita sem qualquer apoio externo não explicitamente autorizado. Os resultados, ideias, parágrafos, ou outros extratos tomados de ou inspirados em trabalhos de outros autores, e demais referências bibliográficas usadas, são corretamente citados.

Autor - Daniel Pedro Pires Alves Reis

Faculdade de Engenharia da Universidade do Porto

Faculdade de Engenharia da Universidade do Porto

Functionalized gold nanoparticles as anticancer drug delivery systems

Daniel Pedro Pires Alves Reis

Dissertação realizada no âmbito do
Mestrado em Engenharia Biomédica

Orientador: Manuel Álvaro Neto Coelho

Setembro 2015

Resumo

Recentemente, as nanopartículas de ouro têm sido estudadas para diferentes aplicações biomédicas e, também, como promissores sistemas de libertação de fármacos em terapias anticancerígenas.

Neste trabalho, foram sintetizados nanopartículas de ouro e conjugadas com doxorrubicina e um inibidor de tirosina quinase, varlitinib. A doxorubicina é um fármaco utilizado em quimioterapia classificado como uma antraciclina. Este fármaco tem sido aplicado em diferentes carcinomas, tais como o cancro do pulmão, do pâncreas, da bexiga e da mama. Os inibidores de tirosina-quinase são uma classe de agentes quimioterapêuticos que inibem, ou bloqueiam, a enzima tirosina-quinase. As tirosina-quinases são enzimas responsáveis pela activação de muitas proteínas de cascatas de transdução de sinal.

O principal objectivo deste projecto foi o de conjugar ambos os fármacos anti-cancerígenos em nanopartículas de ouro funcionalizadas, com o objetivo de obter uma resposta sinérgica.

Ambos os fármacos anti-cancerígenos foram conjugados com sucesso às nanopartículas, através de um processo sequencial de peguilação (funcionalização de AuNPs com poli (etileno) glicol [PEG]), ativação química do PEG e conjugação dos fármacos.

As nanopartículas de ouro peguiladas (PEGAuNPs) e conjugadas foram sintetizadas e caracterizadas quanto ao seu tamanho (Espalhamento de Luz Dinâmico, Espectroscopia de Absorção), morfologia (Microscopia Eletrônica de Transmissão), estabilidade em solução (Espalhamento de Luz Electroforético) e estrutura química (Fourier Transform Infrared Spectroscopy).

As nanopartículas conjugadas exibem uma libertação controlada dos fármacos anti-cancerígenos, durante 72 horas. Os perfis de libertação foram obtidos por comparação da análise fluorimétrica dos fármacos na presença e ausência das nanopartículas em solução.

Em conclusão, os nanosistemas desenvolvidos podem ser uma alternativa promissora para a terapia do cancro.

Abstract

Recently, gold nanoparticles have been studied for different biomedical applications and, also, as promising delivery systems for cancer treatments.

In this work, gold nanoparticles were synthesized and conjugated with doxorubicin and a tyrosine kinase inhibitor, varlitinib. Doxorubicin is a chemotherapy drug classified as an anthracycline. This anticancer drug has been used in different carcinomas such as non-small cell lung cancer, pancreatic cancer, bladder cancer and breast cancer. Tyrosine-kinase inhibitors are a class of chemotherapy agents that inhibit, or block, the enzyme tyrosine kinase. Tyrosine kinases are enzymes responsible for the activation of many proteins by signal transduction cascades.

The main goal of this project was to conjugate both anticancer drugs to functionalized gold nanoparticles, aiming to reach a synergic.

Both anticancer drugs were successfully conjugated to the nanoparticles, through a sequential process of pegylation (functionalization of AuNPs with poly-(ethylene) glycol [PEG]), PEG chemical activation and drug conjugation.

Pegylated gold nanoparticles with drug conjugation were synthesized and characterized regarding their size (Dynamic Light Scattering, Absorption Spectroscopy), morphology (Transmission Electron Microscopy), stability in solution (Laser Doppler Velocimetry) and chemical structure (Fourier Transform Infrared Spectroscopy).

The conjugated nanoparticles displayed a controlled release of the anticancer drugs, through a 72-hour timeline. The release profiles were obtained by comparing the fluorimetric analysis of conjugated nanoparticles in solution with the drugs alone in suspension.

In conclusion, the nanosystems developed can be a promising alternative for cancer therapy.

Acknowledgments

Firstly, I would like to acknowledge both my supervisor, Prof. Dr. Manuel Coelho and my co-supervisor, Dr. Sílvia Coelho, for their constant support and guidance, but mostly, for believing in me and allowing me to develop and grow as a student, a scientist and a person.

I must also gratefully acknowledge Rui Fernandes from IBMC for the TEM morphologic analysis of the gold nanoparticles.

I gratefully acknowledge funding received from TRANSCAN-FCT (research project TRANSCAN/0001/2012) and Portuguese cancer league.

To my colleagues at DEQ, thank you for making me feel at home since the day I set foot in our laboratory.

A word of thankfulness to each and every one of my friends, for simply being there no matter the circumstances.

And finally, to my parents and my little brother, thank you for making everything I am and have, possible.

Table of Contents

List of figures

List of tables

List of abbreviations

ATR-FTIR	*Attenuated Total Reflectance-Fourier Transform Infrared Spectroscopy*
AuNPs	*Gold Nanoparticles*
Bcr-abl	*Breakpoint Cluster Region-Abl gene*
CycG2	*Cyclin G2*
DLS	*Dynamic Light Scattering*
DMOS	*Dimethyl sulfoxide*
DOX	*Doxorubicin*
EDC	*1-ethyl-3-(3dimethylaminopropyl)-carbodiimide*
EGF-R1	*Epidermal growth factor receptor*
ELS	*Electrophoretic Light Scattering*
EPR	*Enhanced Permeability Retention*
FBS	*Fetal Bovine Serum*
FTIR	*Fourier Transform Infrared Spectroscopy*
LDV	*Laser Doppler Velocimetry*
MnSOD	*Manganese superoxide dismutase*
NPs	*Nanoparicles*
PBS	*Phosphate Buffer Saline*
PDGF-R	*Platelet-derived growth factor receptor*
PEG	*Poly-(ethylene) glycol*
PEGAuNPs	*Pegylated Gold Nanoparticles*
S-NHS	*Sulfo-(N-hydroxysulfosuccinimide)*
TEM	*Tramsission Electron Microscopy*
TKI	*Tyrosine Kinase Inhibitor*
TOP2	*Topoisomerase II*

List of symbols

C	*Concentration*
D_s	*Translational diffusion coefficient*

f(ka)	*Henry function*
k	*Boltzmann's constant*
l	*Distance*
R_h	*Laser hydrodynamic radius*
T	*Absolute temperature*
ε	*Molar absorptivity*
ζ	*Zeta potential*
η	*Viscosity*
μ	*Eletrophoretic mobility*

Chapter 1

Introduction

1.1. Classic cancer therapies and its challenges

With an ever increasingly older population, cancer casts a very large shadow over the world, particularly in developing countries. Whether due to environmental factors or cancer-causing behaviors, such as smoking, the death toll associated with this once considered incurable disease continues to grow. According to the 2008 GLOBOCAN project, it is estimated that about 12.7 million cancer cases and 7.6 million cancer deaths have occurred in 2008. Of these, 56% of the cases and 64% of the deaths occurred in the economically developing world [1].

The sheer volume of this numbers, calls for a constant improvement in both diagnostic and therapeutic approaches. Currently, surgery, chemo and radiotherapy are the leading therapeutic approaches, all of them possessing intrinsic and undesirable side effects. Although surgery and radiotherapy are considered local therapies, chemotherapy acts systemically through the bloodstream. This posts a major issue for such approaches, mostly due to the high toxicity of the antitumoral drugs, their short life-time in the human body and lack of specificity to the tumor site. Many drugs are merely removed in their first blood circulation through the kidney and the liver, breaking apart before reaching their targets. Another problem which is encountered in conventional anticancer drugs is their low solubility, requiring a large amount of drug to be used in order to be effective, which, in most cases exceeds their dose-limiting toxicity, as previously referred [2–6].

Considering the sum of these facts, it is quite obvious that a novel, more targeted and less harmful approach, must be established. For both diagnostic and therapeutic approaches, nanomedicine may have come up with a solution: nanoparticles. In this study a specific category of nanoparticles will be highlighted, gold nanoparticles, as they show great promise and potential in a wide array of clinical applications.

.

1.2. Nanoparticles

Nanoparticles (NPs) are usually smaller than several hundred nanometers in size, comparable to large biological molecules such as enzymes, receptors, and antibodies. With size ranging about one hundred to ten thousand times smaller than human cells, these nanoparticles are able to interact with biomolecules both on the surface of and inside the cells, which may revolutionize cancer diagnosis and treatment. Other features associated with these particles are their unique physicochemical properties such as: small size, larger surface area, stability, varied composition, biocompatibility and biodegradability [7–11]. Through distinct synthesis processes, different types of nanoparticles may be obtained, from dendrimers to liposomes, nanospheres to nanotubes or nanocapsules. Each of these structures has its advantages and disadvantages, and one must take into consideration its features when selecting the nanocarrier for the targeted approach.

Recently, nanoparticles of several types of materials (such as lipids, metals or other compounds) have been studied and regarded as a great alternative for the conventional cancer therapies, or even at a diagnosis level through new bioimaging techniques. Briefly, Table 1 highlights some of the materials used in the preparation of nanocarriers.

Table 1- Nanosystems in drug delivery applications and materials used in its fabrication.

Nanosystem	Materials	References
Dendrimers	Poly(amidoamine);	[12]
Inorganic Nanoparticles	Gold Nanoparticles (AuNPs); carbon nanotubes; silica nanoparticles	[13–15]
Polymer-based Nanoparticles	Poly(ciano)acrylates; Polyethyleinemine; Polysaccharides;	[16], [17]
Lipossomes	Phospholipids;	[18–20]

The main aims of these strategies are to overcome non-cellular and cellular mechanisms of resistance and to boost the selectivity of the drugs towards tumor cells, thus reducing their toxicity regarding normal tissue cells. To deliver therapeutic agents to tumor cells, several problems must be addressed and solved. Firstly, drug resistance at the tumor level due to physiological barriers (non-cellular based mechanisms). Secondly, drug resistance at the cellular level (cellular mechanisms). Finally, the distribution, biotransformation and clearance of anticancer drugs in the system must be assessed. Several studies state that, using nanoparticles as drug delivery or simply as a bioimaging toll, all of these barriers may be overcome [3], [8], [21–23].

To bypass the inherent limitations of the classic cancer therapies, several drug delivery systems have been a part of the edge in scientific research. It is crucial to improve the retention and release of therapeutic and diagnostic agents to overcome the refereed limitations [14], [15].

Nanoparticles are considered the gold standard of drug delivery nanosystems, due to their aforementioned intrinsic characteristics. By encapsulating drugs in a nanoparticle, the drug's bioavailability and bioaccumulation in the target site will improve, decreasing its toxicity. The fulfillment of these main goals allows maximizing therapeutic effects and minimizing side effects. These goals are achieved by drug encapsulation itself, but also by modifying NPs' surface. The encapsulation of the drug minimizes its premature degradation after administration, since it allows protection and stabilization of the drug against environmental or biological factors. This drug increased stability promotes an enhancement in its bioavailability. Also, in order to increase the bioavailability of the drug, the functionalized NP allows overcoming the biological barriers that would lead to its elimination. The toxicity of the drug is also reduced since NPs allows the use of lower doses, since the delivery may be localized rather than systemic. Also a decrease in toxicity is due to the drug being less likely to act on healthy cells, since it is possible to guide the NPs to the diseased tissues, increasing accumulation in the target tissues, through the Enhanced Permeability and Retention (EPR) effect (Figure 1).

The EPR effect is a unique phenomenon of solid tumors based on their anatomical and pathophysiological differences from healthy tissues. Since angiogenesis leads to high vascular density in solid tumors, large gaps exist between endothelial cells in tumor blood vessels, and tumor tissues show selective extravasation and retention of macromolecular drugs or even nanoparticles [22], [24]–[27]. This EPR effect served as a basis for development of several anticancer nanoparticle therapies.

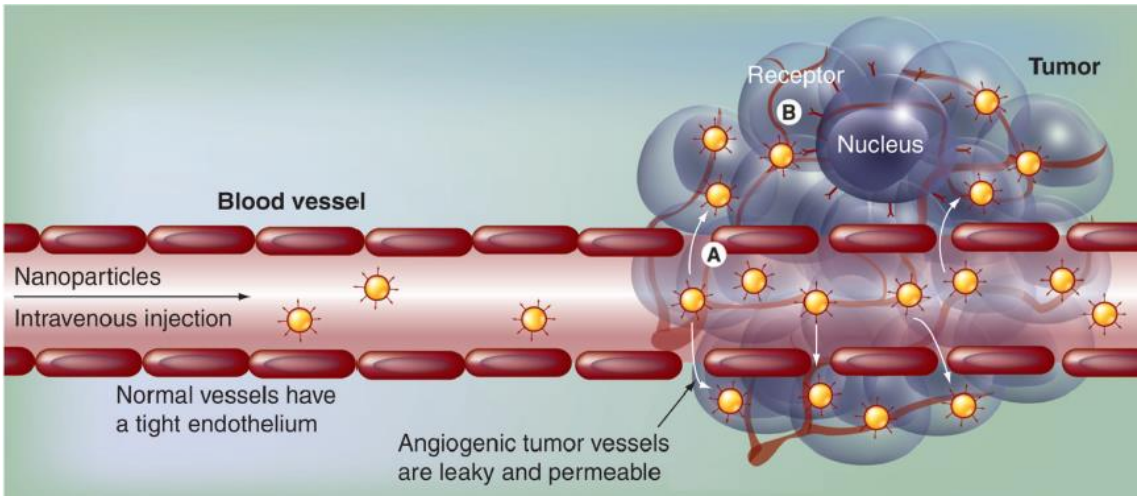

Figure 1-Enhanced drug delivery to solid tumors using nanoparticles: (A) Passive targeted delivery. (B) Active targeted delivery [27].

1.2.1 Gold Nanoparticles

Gold nanoparticles (AuNPs) with controlled geometrical, optical, and surface chemical properties are the subject of intensive studies and applications in biology and medicine. Presently, there is a wide diversity of published examples which includes genomics and biosensorics, immunoassays and clinical chemistry, photothermolysis of cancer cells and tumors, targeted delivery of drugs and antigens, and optical bioimaging of cells and tissues with nanophotonic detection systems [8].

There are several ways to synthesize AuNPs with most of them starting from commercial $HAuCl_4$. Citrate reduction of Au^{III} to Au^0 in water was introduced by Turkevitch et al. in 1951, a method that is still used nowadays to subsequently replace the citrate ligand of these AuNPs by appropriate ligands of biological interest [10], [28]. Recent modifications of the Turkevitch method have allowed better size distribution and size control within the 9–120 nm range [6], [29]. AuNPs can be stabilized by a large variety of stabilizers (ligands, surfactants, polymers, dendrimers or biomolecules), allowing for an even broader diversity of these particles. However, it has been established that the most robust AuNPs were developed by Giersig and Mulvaney through stabilization by thiolates using the strong Au–S bond between the soft acid Au and a soft thiolate base [30]. In figure 2, several different types of gold nanoparticles are represented.

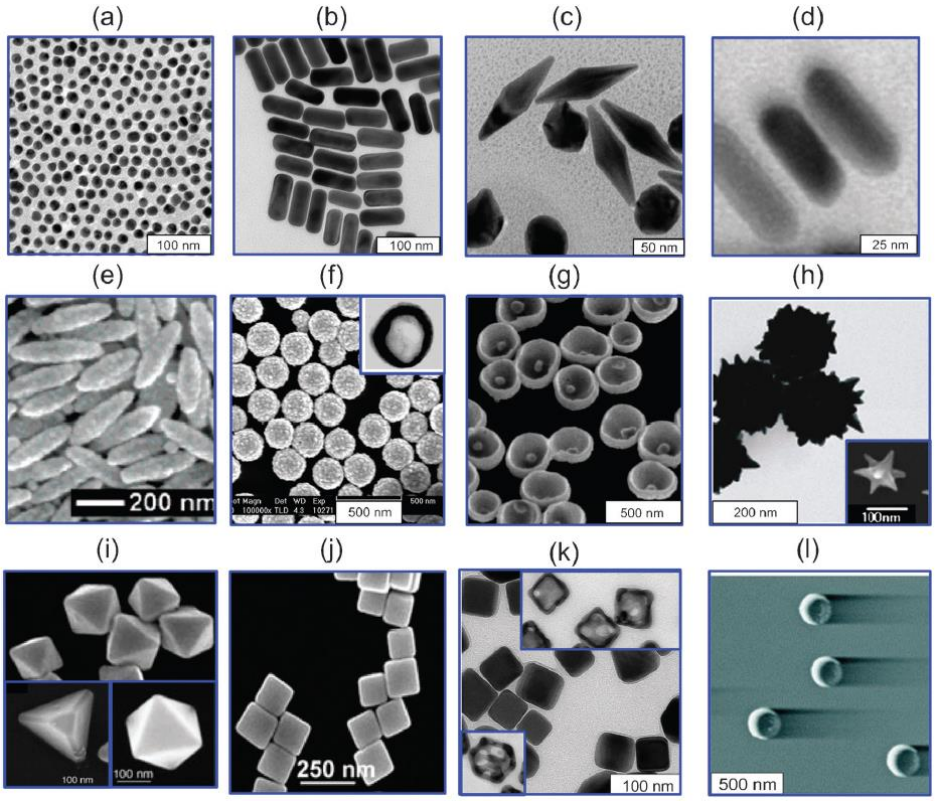

Figure 2-Various types of plasmon-resonant nanoparticles: 16 nm nanospheres (a); gold nanorods (b); gold bipyramids (c); gold nanorods (d); ''nanorice'' (gold-coated Fe_2O_3 nanorods) (e); SiO_2/Au nanoshells (f) (the inset shows a hollow nanoshell); nanobowls with bottom cores (g); spiky SiO_2/Au nanoshells (h) (the inset shows a gold nanostar); gold tetrahedra, octahedra, and cubooctahedra (i); gold nanocubes (j); silver nanocubes and gold–silver nanocages obtained from them (in the insets) (k); and gold nanocrescents (l)[8].

A unique feature of this solution is its color oscillation, which is directly correlated with the size of the particles in suspension. This feature is a reflection of the Surface Plasmon Band, a physical property described as a broad absorption band in the visible region around 520 nm. Smaller particles provide a deep-red color, while increasingly larger ones lead to a shift the absorption peak to higher wavelengths, giving the solution a purple hue [5], [10].

Due to its unique characteristics, AuNPs may be applied to both diagnostics and therapy (Figure 3). Several studies describe these particles as a bioimaging tool and, historically, electron microscopy (mainly transmission electron microscopy [TEM]) has for a long time been the principal method to detect specific biological interactions with the help of colloidal gold particles in suspension (due to their high electron density)[8], [31]. Concerning its therapetuical applications, photothermal or photodynamic approaches are frequently found in clinical situations. Most recently, several research groups associate or conjugate drugs or genes to AuNPs, acting as a drug delivery agent [4], [5], [32].

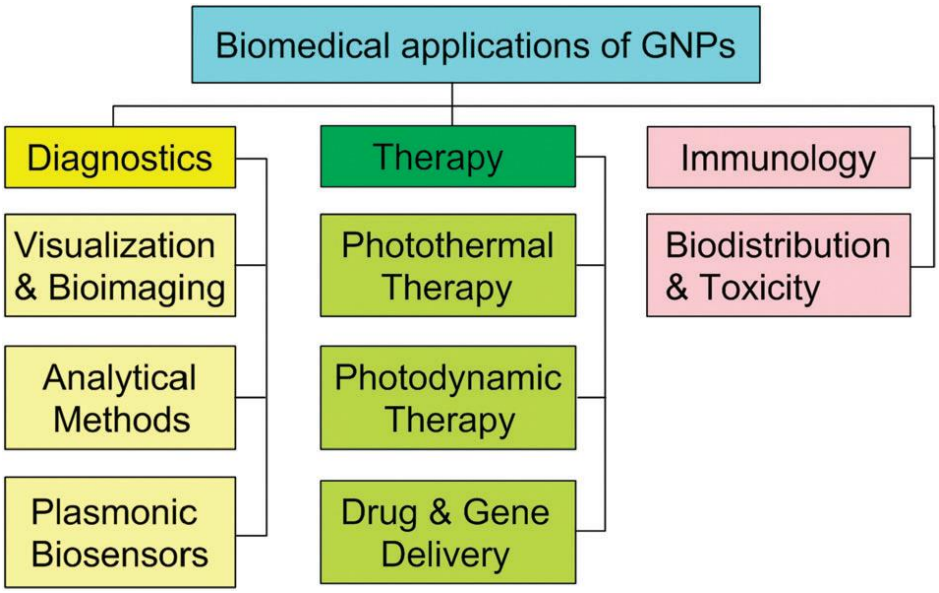

Figure 3- Generalized scheme for the biomedical application of gold nanoparticles (AuNPs). Along with basic applications in diagnostics and therapy [8].

As previously mentioned, there is an enhanced retention of the particles in tumor tissue, leading to an accumulation in such sites. Due to its small size, AuNPs are easily internalized by tumor cells, via lysosomes. Here, alterations in pH values lead to an increased release of therapeutic agents, when conjugated to the particles. Such reaction greatly decreases the necessary drug concentrations administered to the organism, reducing its side effects, but also increasing the treatment specificity and efficiency. Usually, to enhance the stability and bioavalability of the particles, a poly-(ethylene) glycol (PEG) coating is carried out. PEG coating not only stealths the nanoparticles from the body's immune system but also facilitates the conjugation of several drugs, through the functionalization of the terminal site of the PEG molecule [5], [33].

Despite its innate potential for bioimaging, AuNPs have also been intensively studied as a therapeutic agent and have been developed as effective carriers for drug delivery because of their high tissue permeability, high colloidal stability, and small size. Several clinical trials applying this colloidal system exist, particularly for pancreatic, ovarian and breast cancer, melanoma and multiple myeloma [3–5], [11], [32], [34].

There is a vast array of chemotherapeutical agents being conjugated to pegylated gold nanoparticles (PEGAuNPs), with promising results. Table 2 briefly resumes the current applications of these systems.

Table 2- Antitumor substances conjugated with AuNPs [4], [8], [35], [36]

Drugs	Size	Functionalization	Cell lines
Paclitaxel	AuNPs, 26 nm	PEG–SH as a linker	MC-38; C57/BL6 mice implanted with B16/F10; melanoma cells
Oxaliplatin	AuNPs, 30 nm	PEG–SH as a linker	A549, HCT116, HCT15, HT29, RKO
Tamoxifen	AuNPs, 25 nm	PEG–SH as a linker	MDA-MB-231, MCF-7, HSC-3
b-Lapachon	AuNPs, 30 nm	PEG–SH as a linker	MCF-7
Doxorubicin	AuNPs, 12 nm	Physical adsorption	KB
Cisplatin	AuNPs, 5 nm	PEG–SH as a linker	OV-167, OVCAR-5, HUVEC, OSE
Bortezomib	AuNPs, 20 nm	PEG–SH as a linker	Du145
Afatinib	AuNPs, 20 nm	PEG–SH as a linker	S2-013, A549

1.3. Doxorubicin and its role in cancer therapy

Doxorubicin (DOX) is an antibiotic anthracycline, a class of drugs derived from *Streptomyces* bacterium *Streptomyces peucetius*. This class of drugs is perceived as the most effective anticancer treatment developed and is effective against a wide range of cancer phenotypes, especially when compared to other class of chemotherapeutic agents [37], [38]. Doxorubicin's *modus operandi* consists of an inhibition of the synthesis of DNA by intercalating into the DNA strand, by interference in the activity of DNA topoisomerase II (TOP2). It is at the peak of its activity in cells undergoing rapid proliferation and are expressing high levels of TOP2 [39]. Other effects have been associated to this drug, such as cell apoptosis triggered by ceramide production, increased free radical production and even cell-cycle checkpoint arresting [39], [40].

Having so many distinct effects on cellular behavior, Doxorubicin has been extensively studied in several *in vitro* researches. A work developed by Zimmermman *et al*. claims that doxorubicin induced G2/M checkpoint arrest by elevating cyclin G2 (CycG2) expression and phospho-modification of proteins in the ataxia telangiectasia mutated signaling pathways [41]. Mandili *et al*. treated neuroblastoma cells with nanomolar doxorubicin, causing dose-dependent over-ubiquitination of a specific set of proteins, indicating that Doxorubicin may also exert its effect through protein damaging [42].

Some *in vivo* studies have already been carried out, using doxorubicin in association with other compounds. For example, a study combining doxorubicin with adenoviral manganese superoxide dismutase (MnSOD) lead to a decrease in MB231 tumors and prolonged survival, in mice [43]. There is also a Phase III clinical trial in subjects with locally advanced unresectable or metastatic soft tissue sarcoma.

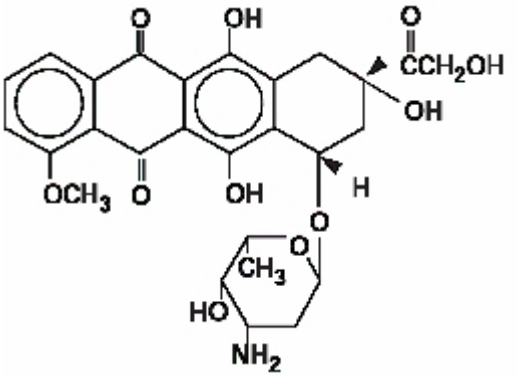

Figure 4- Chemical structure of doxorubicin (Adriamycin)[38].

1.3.1 Gold Nanoparticles as Doxorubicin carriers

Some research groups have already established systems with doxorubicin conjugated to gold nanoparticles, with variations regarding both the conjugation reaction and the final conjugate structure. The most common and efficient process, although, is through PEG functionalization with cross-linking reagents such as 1-ethyl-3-(3dimethylaminopropyl)-carbodiimide (EDC) and Sulfo-N-hydroxysulfosuccinimide (NHS). This reaction greatly increases the PEGAuNPs susceptibility to link with other compounds. Figure 5 briefly summarizes the standard conjugation reaction.

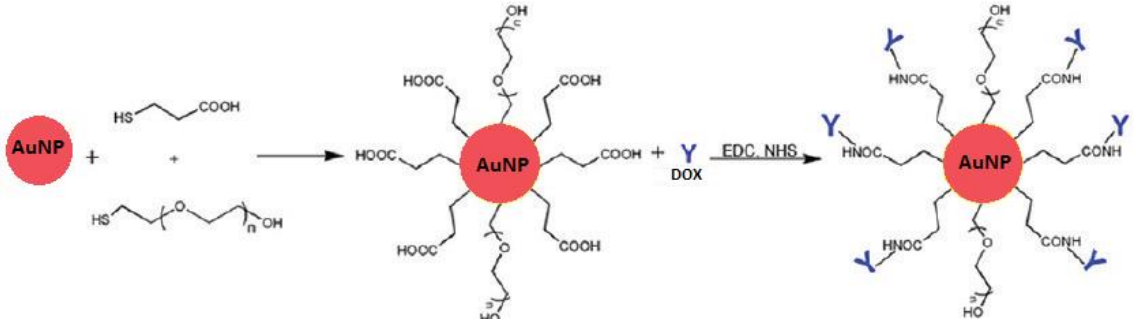

Figure 5-Template for the usual conjugation reaction between PEGAuNPs and doxorubicin.

PEG itself lacks reactivity towards biochemical agents, an advantage for the particles stability, but a drawback regarding its functionalization. Another pathway to ensure the drug's conjugation to the particles it's the functionalization of the drug itself, instead of the NPs. For example, through thiolation of DOX, a research group was able to successfully conjugate the drug to pegylated gold nanoparticles. One of the drawbacks of such approach might reside in the attenuation of the drug's bioactivity by structural alterations [4]. Finally, another approach to ensure the functionalization of the AuNPs is via a direct ligand between the PEG chain and the

molecule of interest. Some of the chosen compounds for this task are hydrazine or folic acid [5], [21].

Some *in vitro* studies have been developed to access the potential of gold nanoparticles in conjugation with doxorubicin. According to Spadavecchia *et al.,* due to its interaction with DNA chains, DOX-conjugated AuNPs may be considered a useful tool to detect, in a sensitive manner, DNA hybridisation events [44]. Another important characteristic of such conjugates has been reported by Aryal *et al.*, claiming that this nanoparticles show a pH-responsive release of the antitumoral drug, a vital feature for these drug nanocarriers [21]. More recently, a work developed by Elbialy *et al.*, concluded that, in presence of a suitable external magnetic field, the administration of DOX-conjugated gold nanoparticles presents the best therapeutic anticancer activity and lowest systemic toxicity when compared to that of free DOX [45].

1.4. Tyrosine-kinase inhibitors in chemotherapy

Conventional chemotherapy, despite being directed toward certain macromolecules or enzymes, typically does not discriminate effectively between rapidly dividing normal cells (e.g., bone marrow and gastrointestinal tract) and tumor cells, leading to several undesired toxic side effects. Tumor responses from cytotoxic chemotherapy are usually unpredictable. To overcome this obstacle, targeted therapies interfering with molecular targets that have a role in tumor growth or progression emerged as a solution. These targets are usually located in tumor cells, although some (e.g. antiangiogenic agents) may target other cells such as endothelial cells. There are multiple types of targeted therapies available, including monoclonal antibodies, inhibitors of tyrosine kinases, and antisense inhibitors of growth factor receptors. Tyrosine kinase inhibitors (TKI) are effective in the targeted treatment of various malignancies via the competitive ATP inhibition at the catalytic binding site of tyrosine kinase. These compounds present several side effects on skin and hair such as folliculitis, paronychia, facial hair growth, facial erythema, and varying forms of frontal alopecia [46–48]. A resumed overview of some inhibitors being studied is displayed in table 3.

Table 3-Overview of Tyrosine inhibitors as Therapeutic Targets [46].

	Imatinib	Dasatinib	Nilotinib	Sunitinib	Sorafenib	Pazopanib	Lapatinib
Bcr-abl	+	+	+				
c-kit	+	+	+	+	+	+	
PDGF-R	+	+	+	+	+	+	
EGF-R1				+			+

Associating these factors with an already selective (although indirect) methodology like nanoparticles may represent a step forward in cancer treatment. Not only will it reduce the side effects of the inhibitors but also guide the particles towards cells that are overexpressing the targeted proteins, which is the case of tumor cells [47], [49].

1.4.1 Varlitinib

Varlitinib (Figure 4) is a selective and potent ErbB1 and ErbB2 inhibitor and functions as a reversible ATP-competitive inhibitor with nanomolar potency (Ki=1 nM) both in vitro and in cell-based proliferation assays using A431 and BT-474 cells. It is an AKT pathway inhibitor in cells that contains active ErbB-2 receptors. It also suppresses ErbB-2 and ErbB-1 phosphorylation in human cancer cells, such as BT-474 and that overexpress ErbB-2 and ErbB-1, respectively. When dosed orally, ARRY-334543 inhibits growth of human tumor xenografts that overexpress ErbB-1 (A431) or ErbB-2 (MDA-MD-453) in a dose-dependent manner. This activity is superior to that seen with a benchmark compound [50]. Based on potency, selectivity and efficacy data, the compound is currently in development as an anti-cancer agent.

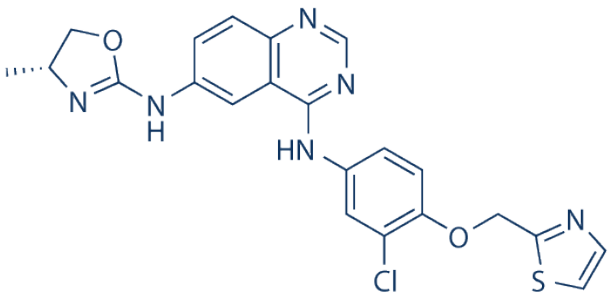

Figure 6 - Varlitinib chemical structure [50]

Chapter 2

Materials and Methods

2.1. Materials

Doxorubicin and varlitinib were purchased from Selleck Chemicals LLC (USA). Sodium citrate, tetrachloroauric (III) acid ($HAuCL_4$; 99.99% trace metal basis, 30 wt% in dilute HCl) and dimethyl sulfoxide (DMSO) were purchased from Sigma-Aldrich (Germany). Phosphate buffered saline (PBS: 0.01 M, 0.0027 M KCl, 0.137 M NaCl, pH 7.4) was purchased from Sigma-Aldrich (Germany). α-thiol-ω-carboxyl (polyethylene glycol) (molecular weight 394.57 Da) was purchased from Prochimia (Poland). Sulfo-NHS (N-hydroxysulfosuccinimide, molecular weight 217.3 Da) was purchased from Fluka (Germany). 1-ethyl-3-(3dimethylaminopropyl)-carbodiimide (EDC, molecular weight 191.7 Da) was purchased from Sigma-Aldrich (Germany).

2.2. System

2.2.1. Pegylated gold nanoparticle synthesis

Gold Nanoparticles (AuNPs) were synthesized by reduction of $HAuCl_4$ using sodium citrate, a process based on the Turkevich-Frens method [29] [30]. $HAuCl_4$ aqueous solution was heated to its boiling point and stirred. Trisodium citrate was swiftly added and boiled during 12 minutes. Finally, the solution was allowed to cool off for posterior functionalization. Pegylation of AuNPs (PEGAuNPs) was achieved through addition of α-thiol-ω-carboxyl polyethylene glycol (PEG) capped with carboxylate group at a molar ratio of 1:1000. The mixture was stirred at room temperature for approximately 1 hour. The final solution was centrifuged at 13400 rpm during 10 minutes and the pellet was ressuspended in water, to remove the unbound PEG molecules. The concentration of the PEGAuNPs was determined by the Lambert-Beer Law assuming the molar absorptivity of the particles plasmon resonance band at 526 nm being $2.33 \times 10^8\ M^{-1}\ cm^{-1}$ [51].

2.2.2. Conjugation of Doxorubicin to PEGAuNPs

Doxorubicin stock solution was prepared in DMSO at room temperature [1mM], and dilutions were performed by addition of water to obtain the desired concentrations. EDC and S-NHS were used as reagents to functionalize the PEG layer in the AuNPs, thus increasing its reactivity towards the drug. To conjugate doxorubicin to the gold nanoparticles, firstly, EDC was added to 6 ml of PEGAuNPs solution and stirred at room temperature. Secondly, S-NHS was added but with a reaction time of 5 minutes. After, 1 mL of doxorubicin in solution was added, with an estimated reaction time of 4 hours, at room temperature and constant stirring. The ratios for the reaction were: EDC and S-NHS at 1:4 molar ratio and 1:1 of doxorubicin, both regarding PEG. To remove the unbound drug, and estimate the conjugation efficiency of the process, the resulting solution was centrifuged at 13000 rpms during 10 minutes and most of the supernatant was discarded and replaced with water.

2.2.2. Conjugation of Varlitinib to PEGAuNPs

Varlitinib stock solution was prepared in DMSO at room temperature [1,5mM], and dilutions were performed by addition of water to obtain the desired concentrations. EDC and S-NHS were used as reagents to functionalize the PEG layer in the AuNPs, increasing its reactivity towards the drug. To conjugate varlitinb to the gold nanoparticles, firstly, EDC was added to 6 ml of PEGAuNPs solution and stirred at room temperature and, secondly, S-NHS was added. Finally, 1 mL of varlitinb in solution was added, with an estimated reaction time of 4 hours, at room temperature and constant stirring. The ratios for the reaction were: EDC and S-NHS at 1:4 molar ratio and 1:1 of varlitinb, both regarding PEG. To remove the unbound drug, and estimate the conjugation efficiency of the process, the resulting solution was centrifuged at 13000 rpms during 10 minutes and most of the supernatant was discarded and replaced with water.

2.3. Methods

2.3.1. Dynamic Light Scattering (DLS)

Dynamic Light Scattering is a method used to determine the size of particles in a solution and their size distribution in dispersion. It measures the intensity of the dispersed light by a molecule or particle through time. Temperature and viscosity of the sample must be known as these factors will disturb or alter the dynamic behavior of the particles, leading to misinterpretations of their size. This method is also vital to infer any alteration in the particle's surface, since any change will affect its diffusion speed [52].

The incident light from the laser will be scattered by any particles in the solution. If the particles are static, the amount of scattered light will remain constant. But, if they are in constant motion, as it's the case of nanoparticles in suspension (Brownian movements), the light intensity will vary. By measuring the variations of light intensity through time, DLS provides information on average particle size and size distribution in suspension. The rate of change of scattered light is directly proportional to the movement of the particles and can be related to their diffusion coefficient. Then, NPs size can be calculated from the diffusion coefficient, using Stokes-Einstein equation:

$$Ds = \frac{kT}{6\pi\eta Rh}$$

where R_h is Laser hydrodynamic radius of the scattering particle; D_s is the translational diffusion coefficient, which depends on the size of the particle, on the surface structure and on the concentration and type of ions in solution; k is the Boltzmann's constant; T is the absolute temperature and η is the viscosity [53].

The hydrodynamic diameter of the particles in suspension was analyzed by dynamic light scattering (DLS) using a Zetasizer Nano ZS (Malvern Instruments Ltd, Malvern, UK), at a constant

temperature of 25ºC. Size measurements were performed at a scattering angle of 173° in a 12 mm^2 polystyrene cuvette (Sarstedt, Germany).

2.3.2. Zeta potential

Electrophoretic light scattering (ELS), also known as Laser Doppler Microelectrophoresis, is used to infer the zeta potential (ζ –potential), a fundamental parameter that describes the electrostatic interactions between particles in a dispersion and its stability. Particles in a suspension attract ions to their surface. These ions form an electrical double layer covering the particle surface. This double layer consists of an inner layer, the Stern layer where counterions are strongly adsorbed, and an outer layer, where ions diffuse more freely. This diffuse layer defines the boundary of the particle as a single charged unit and the electric potential that exists at this boundary is called the zeta potential. Particles with very positive or very negative ζ –potential will repel each other and avoid aggregation. On the other hand, low absolute zeta potential values results in aggregation and flocculation. A physically stable nanosuspension will have a minimum zeta potential of absolute value of 30 mV [54].

Electrophoresis is an electrokinetic effect based on the movement of the particles when submitted to an electric field. Forces related to the particles viscosity will tend to oppose such movement, and when equilibrium is reached between these two opposing forces, the particles move with constant velocity. The velocity will depend on several factors: viscosity (η), zeta potential, the dielectric constant (ε) and the electrophoretic mobility (μ_E). Henry's Law correlates the zeta potential and the electrophoretic mobility [55]:

$$\mu E = \frac{2\varepsilon.\zeta.f(ka)}{3\eta}$$

where μ is the eletrophoretic mobility; ε, the dielectric constant of the dispersant; ζ, the zeta potential; f(ka), is the Henry function and η, the viscosity coefficient.

Identically to the Dynamic Scattering Light, the ZetaSizer Nano ZS was the instrument used to obtain measurements of zeta potencial by ELS. Folded capillary cells from Malvern (Worcestershire, UK) were used and the dispersant medium was water. Mean values for each preparation were obtained by triplicate measurements.

2.3.3. Absorption Spectroscopy

To estimate the concentration of gold nanoparticles in solution from UV absorvance (A) at around 526 nm, calculations using the Lambert-Beer law were performed:

$$A = \varepsilon.C.l$$

where l is the distance through the sample; C is the concentration of the absorbing species and ε is a constant known as the molar absorptivity, which is a molecular property in a given solvent at a specific temperature and pressure.

Spectrums of PEGAuNPs and DOXPEGAuNPs were obtained by UV-Vis absorption using a 1 cm quartz cuvette, at room temperature by a Shimadzu UV-1700 PharmaSpec spectrophotometer.

2.3.4. Fourier Transform Infrared Spectroscopy (FTIR)

Infrared Spectroscopy is a technique that provides information regarding the chemical composition of a material through the identification of its functional groups. It uses low energy radiation, to avoid sample damage, by emission of its electrons [56]. Each functional group vibrates after absorbing a specific wavelength, which frequency corresponds to specific molecular energy levels. By analyzing the sample reflectance and transmittance on the infrared region at different frequencies, a FTIR spectrum is outlined [57].

The AuNPs, PEGAuNPs, DOXPEGAuNPs and VarlitinibPEGAuNPs solutions were analyzed by Attenuated Total Reflectance-Fourier Transform Infrared Spectroscopy (ATR-FTIR). The samples were centrifuged during 15 minutes at 14500 rpms, in order to obtain a dense pellet to minimize water-associated interference in the readings. ATR-FTIR spectra were recorded with an ALPHA FTIR Spectrometer (Bruker) in the spectral range 4000-400 cm^{-1}, resolution of 4 cm^{-1} and 40 scans, at room temperature.

2.3.5. Fluorescence

Fluorimetry consists of a technique used in the study, both quantitatively and qualitatively, of substances through a fluorescent phenomenon, resulting from the absorption of radiant energy and posterior emission of a portion of such energy. The major advantages of this technique are its superior sensitivity when compared with UV-vis spectroscopy (about 100 times more sensitive) and higher selectivity, since not all substances that absolve electromagnetic radiation are capable of emitting fluorescence. The latter may also be regarded as a limitation to the method, restringing the array of substances that can be studied [58], [59].

Both conjugated nanosystems used in this work, with doxorubicin and varlitinib, were quantified through fluorescence measures. Conjugation efficiency, compound stability and *in vitro* release studies all rely on this methodology to achieve viable results. The excitation and emission wavelengths were as followed: for doxorubicin, λ_{ex}=485 nm and λ_{em}= 520 nm; and for Varlitinib λ_{ex}=360 nm and λ_{em}= 485 nm. Fluorescence measures of AuNPs and PEGAuNPs were also performed for these wavelengths, as negative control.

2.3.5.1. Stability studies

As previously mentioned, fluorescence measurements are considered a viable manner to verify the stability or structural integrity of several compounds. Solutions with a known

concentration (approximately 8μM) of both doxorubicin and varlitinib were prepared at room temperature and kept at 37 ºC during 72 hours. Fluorescence readings were carried out at several timepoints during this period, to verify the stability of the anticancer drugs at body temperature.

2.3.5.2. *in vitro* Drug release studies

In vitro drug release studies of doxorubicin and varlitinib conjugated PEGAuNPs were carried out at 37 ºC by dialysis using a regenerated cellulose membrane (molecular weight cut off, MWCO: 8 kDa, purchased from Spectrum Labs Europe BV, Netherlands). Initial conjugated-PEGAuNPs concentration was of approximately 8 nM, and the solutions were incubated in 4 mL of PBS 0.01 M, with constant magnetic stirring.

The drug concentrations in the dialysate buffer were analyzed through time using fluorimetric analysis at the λ_{ex}=485 nm and λ_{em}= 520 nm for doxorubicin and λ_{ex}=360 nm and λ_{em}= 485 nm for varlitinib.

2.3.6. Transmission Electron Microscopy

Transmission electron microscopy (TEM) is arguably the most efficient and versatile technique to characterize the morphology of nanomaterials. This technique has a much higher resolution when compared with other microscopic tools, such as light microscopy and is based on the interaction of an electron beam with the sample through which it passes. When the beam contacts with the sample, electrons will interact with it, and part of them may be transmitted through the sample. These transmitted electrons are captured and focused onto a phosphor screen at the bottom of the microscope where the image is outlined. The beam that reaches the phosphor screen consisted of different amounts of electrons that pass through particular regions of the sample and this difference is what causes the image contrast. Darker areas of the image represent the regions of the sample through which fewer electrons were transmitted, due to the greater thickness or density. On the other hand, brighter areas are the result of increased electronic transmission through the sample, representing thin regions of the sample [60], [61].

The morphological examination of the NPs was performed by TEM Yeol Yem 1400 at an accelerating voltage of 80kV (Tokyo, Japan). For that purpose, the samples were prepared with negative staining. 5 μL samples were stained with 2% (v/v) uranyl acetate for 45 seconds, immobilized on copper grids (Formvar/Carbon on 400 mesh Cu (50) from Agar Scientific), and air-dried for TEM visualization. TEM samples must be prepared in order to improve their visualization. Uranyl acetate is a heavy metal salt capable of scattering electrons, leading to an enhancement in the image contrast [62].

Chapter 3

Results and Discussion

3.1. Gold Nanoparticles Characterization

Gold Nanoparticles (AuNPs) were synthesized by reduction of $HAuCl_4$ using sodium citrate, a process based on the Turkevich-Frens method and posteriorly functionalized with PEG [29]. The size distribution and zeta potential of the PEGAuNPs was determined by Dynamic light scattering (DLS) and Laser Doppler velocimetry (LDV), respectively. The influence of the pegylation was evaluated through the analysis of physicochemical properties of the produced AuNPs and PEGAuNPs with the results being presented in table 4 (n=8).

Table 4-Zeta potential and mean hydrodynamic diameter values for both AuNPs and PEGAuNPs.

	Hydrodynamic diameter (nm)	**Zeta Potential (mV)**
AuNPs	18±6	-37±9
PEGAuNPs	22±7	-41±7

The results in table 4 clearly indicate a slight increase in the hydrodynamic diameter and zeta potential through PEG-functionalization. The particles size increased due to the covalent attachment of PEG polymer chains, which translates in a lower affinity towards other particles in suspension leading to an increasingly negative zeta potential value, conferring stability to colloidal suspension.

The particles in suspension were also be evaluated through TEM, as shown in Figures 7-A and 7-B.

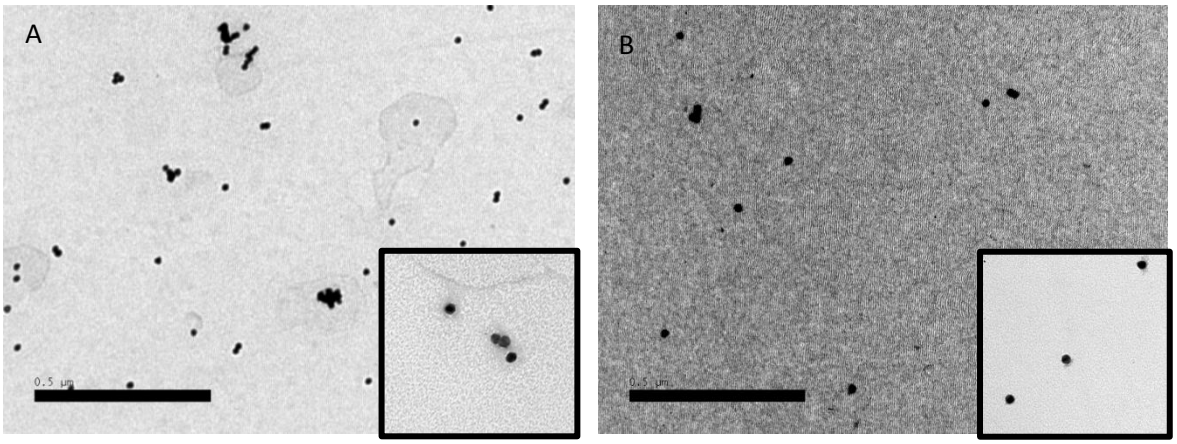

Figure 7-TEM analysis of: a) AuNPs; b) PEGAuNPs. Scale bar is 0.5 μm.

TEM analysis of both AuNPs and PEGAuNPs show the nanoparticles in spherical shape and a size range of approximately 20nm that is in agreement with DLS measurements. It is also possible to observe the low degree of aggregation of the nanoparticles in suspension.

Furthermore, FTIR analysis was carried through to evaluate the chemical structure of both AuNPs and PEGAuNPs, and to confirm that pegylation of the particles was indeed achieved (Figure 8).

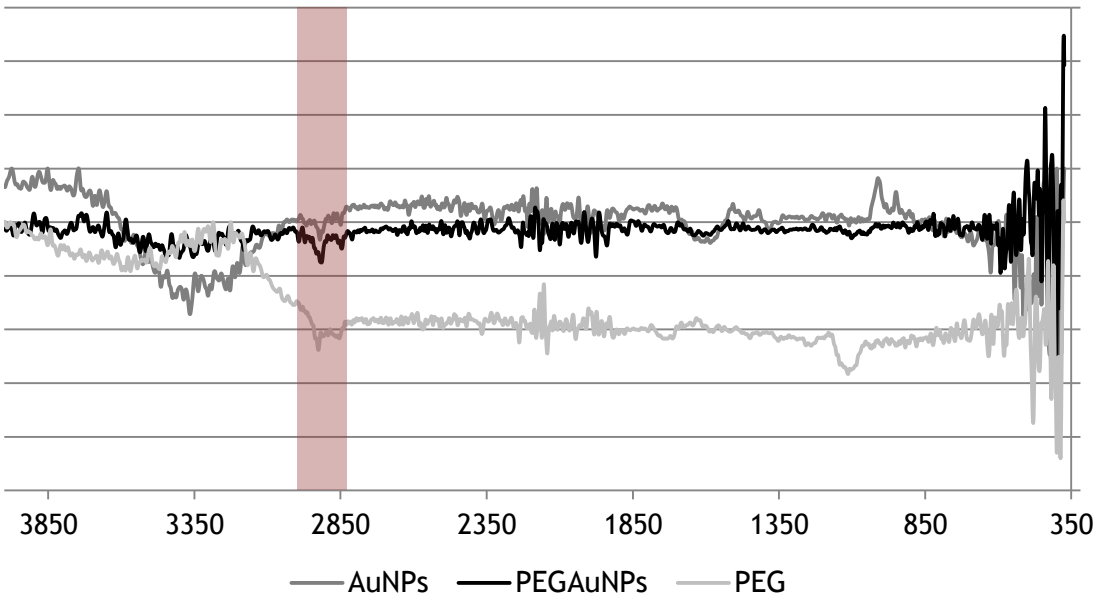

Figure 8-FTIR spectra of gold nanoparticles (AuNPs), pegylated gold nanoparticles (PEGAuNPs) and PEG in solution.

Figure 8 shows the FTIR spectra of AuNPs, synthesized PEGAuNPs, and pure PEG in solution. In contrast to the spectrum of bare AuNPs, IR transmittance peak is present in the spectrum of PEGAuNPs, and this peak is assigned as follows: 2,850–3,000 cm^{-1}(-CH_2 stretching, highlighted) [28].

3.2. Gold Nanoparticles stability

According to Aryal *et al.*, acidic pH influences the behavior and stability of gold nanoparticles [2]. To determine the influence of this factor in the stability of the NPs, continuous studies at 37ºC in 0.01M PBS buffers with distinct pH values were performed. The results are described in tables 5, 6 and 7.

Table 5 - Zeta potential and Hydrodynamic diameter values for PEGAuNPs in DI water, over a period of 42 days. Hydrodynamic diameter results are presented as mean ± SD (% of total population).

H_2O (pH=7,0)	Hydrodynamic diameter (nm)	Zeta Potential (mV)
Before dilution	22 ± 7	-41 ± 7
0 days	35 ± 6	-39 ± 7
1 day	36 ± 6	-37 ± 6
7 days	32±6	-42 ± 7
14 days	34 ± 6 (59,0%) 318 ± 103 (41,0%)	-38 ± 7
28 days	44 ±7 (77,3%) 312 ± 92 (22,7%)	-36 ± 6
42 days	65 ±12(97,8%) 498 ± 266 (2,2%)	-36 ± 6

Table 6-Zeta potential and mean diameter values for PEGAuNPs at pH 7.4, over a period of 42 days. Hydrodynamic diameter results are presented as mean ± SD (% of total population).

pH = 7.4	Hydrodynamic diameter (nm)	Zeta Potential (mV)
Before dilution	22 ± 7	-41 ± 7
0 days	21 ± 5	-27 ± 5
1 day	24 ± 6 (80 %) 462 ± 104 (20%)	-27 ± 5
7 days	23 ± 6 (100%)	-29 ± 5
14 days	22 ± 6 (50,1%) 411 ± 102 (49,9%)	-30 ± 6
28 days	21 ± 6 (62,1%) 452 ± 121 (37,9%)	-29 ± 5
42 days	20 ± 6 (70,5%) 708 ± 204 (29,5%)	-27 ± 5

Table 7-Zeta potential and mean diameter values for PEGAuNPs at pH 5.3 over a period of 42 days, in pH=5.3 PBS buffer solution. Hydrodynamic diameter results are presented as mean ± SD (% of total population).

pH= 5.3	Hydrodynamic diameter (nm)	Zeta Potential (mV)
Before dilution	22 ± 7	-41 ± 7
0 days	187 ± 47 (84,9%) 21 ± 6 (15,1%)	-26 ± 4
1 day	21 ± 6 (74,2 %) 378 ± 96 (25,8%)	-26 ± 3
7 days	25 ± 6 (66%) 378 ± 100 (34 %)	-25 ± 4
14 days	420 ± 107 (62,8%) 28 ± 6 (37,2%)	-25 ± 4
28 days	24 ± 6 (52,3%) 512 ± 126 (47,7%)	-26 ± 3
42 days	18 ± 5 (59,1%) 701 ± 272 (40,9%)	-24 ± 4

Analyzing the zeta potential values, it is clear that an acidic pH value destabilize the system at a quicker rate, which is an indicator for drug delivery since the particles are internalized through lysosomes, where the pH is quite lower than the biological value of 7.4 [63]. It is also observable that the particles tend to aggregate with time at pH 7.4 and 5.3. An effect clearly more prone to happen in acidic pH, as the hydrodynamic diameter data sustains. Studies at pH=3 were also preformed but, due to the immediate nanoparticle aggregation, the continuous study of the solution could not be performed.

3.3. Conjugation of PEGAuNPs with antitumor agents and *in vitro* Release Studies

In this work, two antitumor of distinct purpose were selected: doxorubicin, a widely used chemotherapy agent and varlitinib, a specific target towards overexpressed receptors in several tumor cell lines.

The methodology used for both NPs preparation was similar. Firstly, a drug calibration curve was obtained through fluorescence readings (data not shown), to facilitate drug quantification in both conjugation efficiency and release studies. Drug stability in 0.01M PBS solution at 37ºC was also assessed. These assays allow the determination of the activity of the drug with time. The stability assays of conjugated PEGAuNPs were performed at 37 ºC and in vitro release experiment were investigated. All assays were performed in triplicate.

3.3.1. Conjugation of PEGAuNPs with Doxorubicin: Dox-PEGAuNPs

A solution of doxorubicin [8μM] was quantified through fluorescence readings, with λ_{ex}=485 nm and λ_{em}= 520 nm. The drug stability assay is presented in Figure 9.

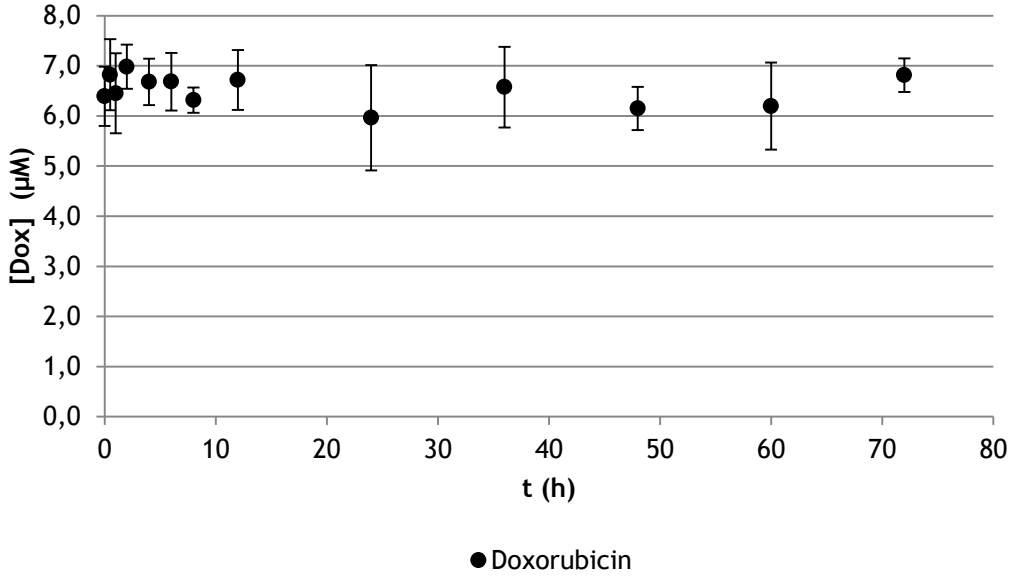

Figure 9 - Doxorubicin stability assay, at 37ºC in PBS.

By analyzing the fluorescence levels of doxorubicin in solution, it is clear that the fluorimetric profile of the drug is stable through time, an indicator of structural integrity of the compound [58].

The conjugation efficiency was determined by fluorimetric analysis of the supernatant of conjugate preparation. The analysis protocol is strictly similar to the one used in the studies regarding doxorubicin. The results for conjugation efficiency and physicochemical analysis are represented in Table 8.

Table 8 - Physico -chemical characterization of-PEGAuNPs and Dox-PEGAuNP

	Hydrodynamic diameter (nm)	**Zeta Potential (mV)**	**Conjugation efficiency (%)**	**Relative [Dox] , μM**
PEGAuNPs	22±7 (100%)	-41±7	-	-
Dox-PEGAuNPs	206±78 (74,6%) 29±10 (22,8%)	-37±6	50±5	≈3,6

According to table 8, it is possible to observe that there is a small, but not significant, decrease in the zeta potential values. The hydrodynamic diameter of the PEGAuNPs changed from 22±7 nm to 29±10 nm. These results indicate some level of interaction between the Dox molecules and the surface of the PEGAuNPs. The conjugation efficiency value was obtained by fluorescence readings the supernatant and it is 50±5%. Therefore, the final concentration of Dox conjugated with PEGAuNPs is determined to be of 3.6 μM.

Additionally, FTIR analysis was performed to evaluate the functionalization of PEGAuNPs with doxorubicin. For reference purposes, analysis of Doxorubicin as a powder was done.

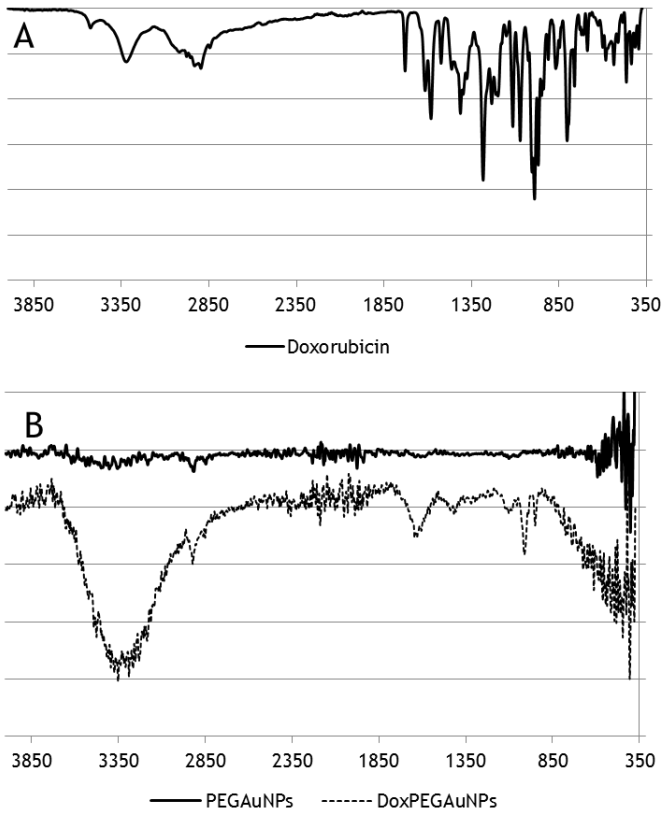

Figure 10-FTIR spectra of: A) Doxorubicin powder; B) Pegylated gold nanoparticles (PEGAuNPs) and Doxorubicin conjugated gold nanoparticles (DoxPegAuNPs).

Figure 10A represents pure doxorubicin, and bands at 1620 cm^{-1}, 1734 cm^{-1} and 2917 cm^{-1} were attributed to N-H bending, C=O stretching vibration and C–H stretching, respectively [45]. Most importantly, for pure DOX, the characteristic band at 3430 cm^{-1} was due to N-H stretching vibrations for primary amine structure [64].

By analyzing Figure 9 B, it is visible that in the case of DOXPEGAuNPs, the amine peak of pure DOX at 3430 cm^{-1} was broadened and a new amide peak at 1050 cm^{-1} appears. They are indicators of a covalent bonding between protonated amine groups of the doxorubicin molecule with the surface of PEGAuNPs, resulting in the formation of an amide [45], [65], [66].

According to FTIR analysis, it could be suggested that DOX molecules were successfully attached to PEGAuNPs surfaces, and that -NH2 group of DOX is the active site for the attachment to the PEGAuNPs.

To determine the stability of the conjugate in near biological conditions, a 37 ºC in PBS study was performed. The hydrodynamic diameter and zeta potential were analyzed to access particle stability. Results are presented in Table 9.

Table 9-Physico-chemical characterization of DOXPEGAuNPs over a period of 72 hours, at 37ºC.

Dox-PEGAuNPs	Hydrodynamic diameter (nm)	Zeta Potential (mV)
0 hours	206 ± 78 (74.6%) 28 ± 10 (25.4%)	-37 ± 6
12 hours	201 ± 74 (71,5%) 25 ± 10 (29.5%)	-34 ±6
24 hours	159 ± 47 (71.8%) 26 ± 10 (28.2%)	-34 ± 6
36 hours	215 ± 68 (74.7%) 24 ± 8 (25.3%)	-33 ± 5
48 hours	145 ± 56 (71.5%) 25 ± 9 (28.5%)	-32 ± 5
72 hours	144 ± 42 (63.3%) 28 ± 12 (32.8%)	-31 ± 6

According to the values depicted in table 9, a small decrease in the zeta potential values is verified. Although it is not enough to consider the particles as unstable in solution since they remain below the -30 mV, a standard value for particle stability [4]. Analyzing the data regarding the nanoparticle's hydrodynamic diameter, it is visible that there is a tendency towards aggregation through time.

To investigate the DOX release conjugated with PEGAuNPs, in vitro release experiments of DOXPEGAuNPs and DOX alone were performed using dialysis membranes (MWCO 8kD) in PBS 0.01 M at 37 ºC. The concentration of DOXPEGAuNPs used was of approximately 10nM (with a relative [DOX]=3.6 μM) and 7.2 μM for DOX solution. The results are shown in Figure 10.

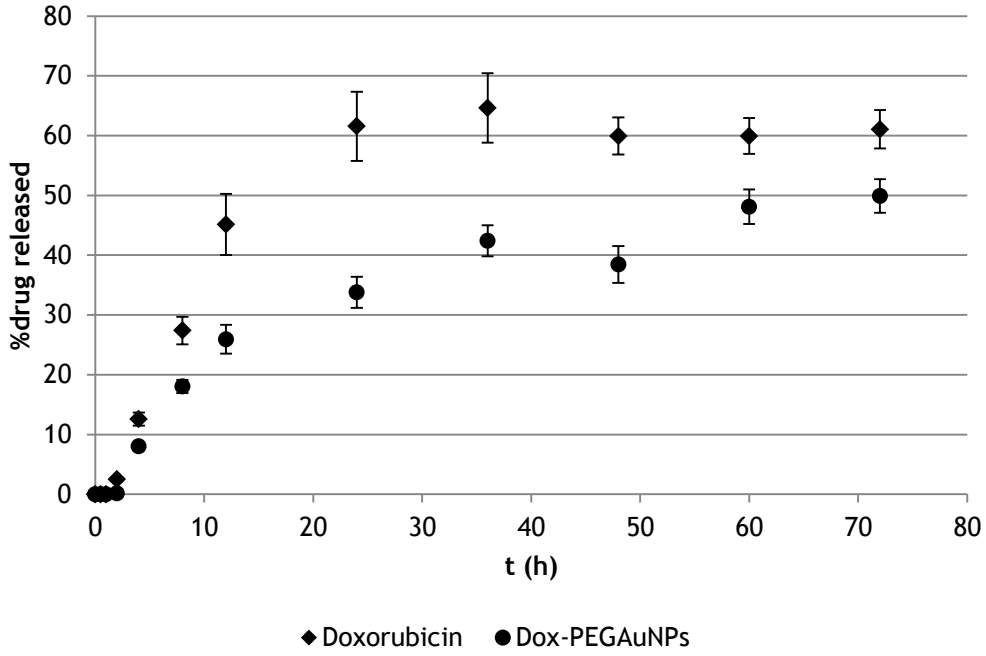

Figure 11-Release profile for Doxorrubicin conjugated PEG-AuNPs

It is observed in Figure 11 a significant gap in Dox release profile in presence of PEGAuNPs when compared to Dox alone. At 24 hours, the amount of Dox released was of 62% and 34% for Dox alone and in combination with PEGAuNPs, respectively. These results suggest some level of interaction between the drug and the surface of PEGAuNPs. After 60 hours, it is visible an arrest in the release of Dox, both in the presence and absence of PEGAuNPs.

3.3.2. Varlitinib-PEGAuNPs

Varlitinib in solution was quantified through fluorescence readings with λ_{ex}=360 nm and λ_{em}= 485 nm. The conjugation efficiency was determined by fluorimetric analysis of the supernatant of conjugate preparation. The analysis protocol is strictly similar to the one used in the studies regarding doxorubicin. The results for conjugation efficiency and physicochemical analysis are represented in Table 10.

Table 10-Physico-chemical characterization of both PEGAuNPs and Varlitinib-PEGAuNPs, conjugation efficiency and relative drug concentration in the conjugate solution.

	Hydrodynamic diameter (nm)	**Zeta Potential (mV)**	**Conjugation efficiency (%)**	**Relative [Varlitinib] µM**
PEGAuNPs	22±7 (100%)	-41±7	-	-
Varlitinib-PEGAuNPs	30±11 (56.2%) 240±101 (43.8%)	-27±8	95±3	≈7

The values presented in table 10 sustain the argument that an interaction occurs between varlitinib and the PEGAuNPs, due to the decrease in zeta potential of the particles. The percentage of conjugated drug with PEGAuNPs is 95±3%. This value indicates an adsorption towards the particles surface, since it is almost undetectable the presence of Varlitinib in the supernatant after the conjugation reaction with PEGAuNPs.

Additionally, FTIR analysis was performed to evaluate the functionalization of PEGAuNPs with Varlitinib. For reference purposes, analysis of Varlitinib as a powder was done.

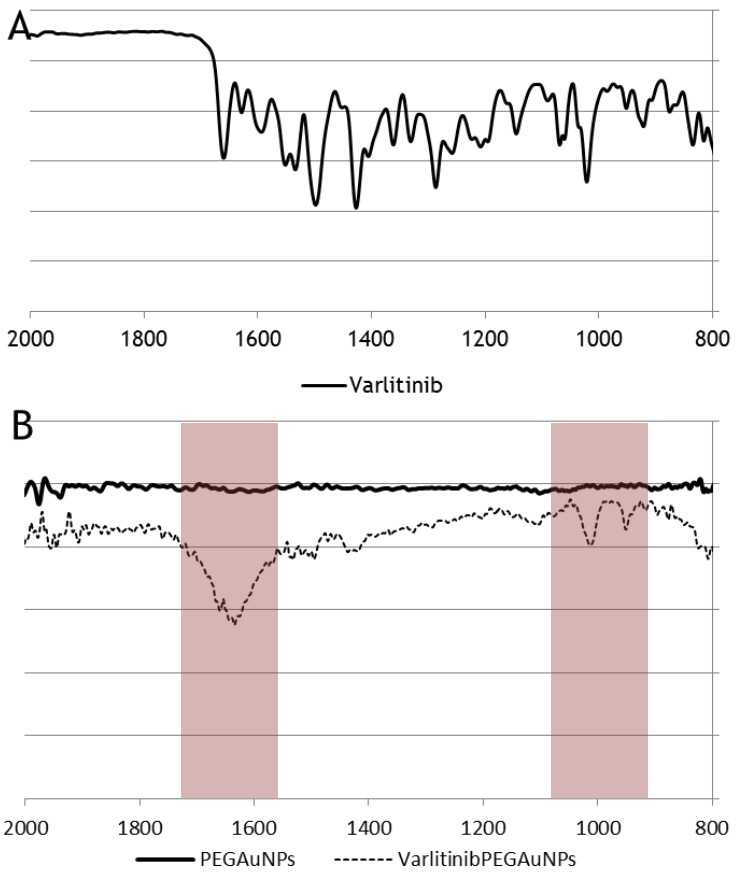

Figure 12-FTIR spectra of: A)Varlitinib powder; B) Pegylated gold nanoparticles (PEGAuNPs) and Varlitinib conjugated gold nanoparticles (Varlitinib-PEGAuNPs).

Figure 12-A represents the FTIR spectra of Varlitinib powder, in which several characteristic peaks are observed. Some of these peaks are concordant to the spectra for VarlitinbPEGAuNPs, and are highlighted in the both spectra. These results clearly indicate the

association of the inhibitor to the nanoparticles, as concluded by comparison of the FTIR spectra of PEGAuNPs and VarlitinibPEGAuNPS (Figure 12-B), sustained by the data acquired through analysis of the drug powder. The characteristic imine peak at 1660 cm^{-1} appears in the FTIR spectra for VarlitinibPEGAuNPs (highlighted in Figure 12-B) , indicating the covalent bond between the secondary amide present in the Varlitinib molecule and the carboxylic group at the end of the PEG chain [36], [66–69]. According to the literature, it is expected to observe an amine characteristic peak at 1100-1000 cm^{-1} which is highlighted in Figure 12-B. This peak is an indicator of the presence of the drug conjugated with the NPs [36].

To determine the stability of the conjugate in conditions approaching the ones in a biological environment, a 37ºC in PBS study was performed. The indicators of particle stability were the hydrodynamic diameter and zeta potential. Results are presented in Table 11.

Table 11-Physico-chemical characterization of Varlitinib-PEGAuNPs over a period of 72 hours, at 37ºC.

Varlitinib-PEGAuNPs	Hydrodynamic diameter (nm)	Zeta Potential (mV)
0 hours	30 ± 11 (56.2%) 240 ± 101 (43.8%)	-27 ± 8
12 hours	200 ± 82 (52.5%) 27 ± 10 (47.5%)	-24 ± 6
24 hours	29 ±11 (55.9%) 243 ± 107 (44.1%)	-24 ± 6
36 hours	25 ± 10 (56.2%) 177 ± 72 (43.8%)	-23 ± 5
48 hours	205 ± 92 (56.7%) 28 ± 10 (43.3%)	-21 ± 5
72 hours	27 ± 11 (59.7%) 142 ± 67 (40.3%)	-17 ± 4

According to the values in table 11, the significant decrease in the zeta potential values show instability in the system after 72 hours of incubation. These values may be a result of a good conjugation efficiency of Varlitinib with PEGAuNPs.

Finally, the *in vitro* drug-release studies were performed at 37ºC in PBS, to evaluate the controlled release of the conjugated therapeutic agent in conditions approaching a biological system. The *in vitro* release profile of the nanocarrier is demonstrated in Figure 13.

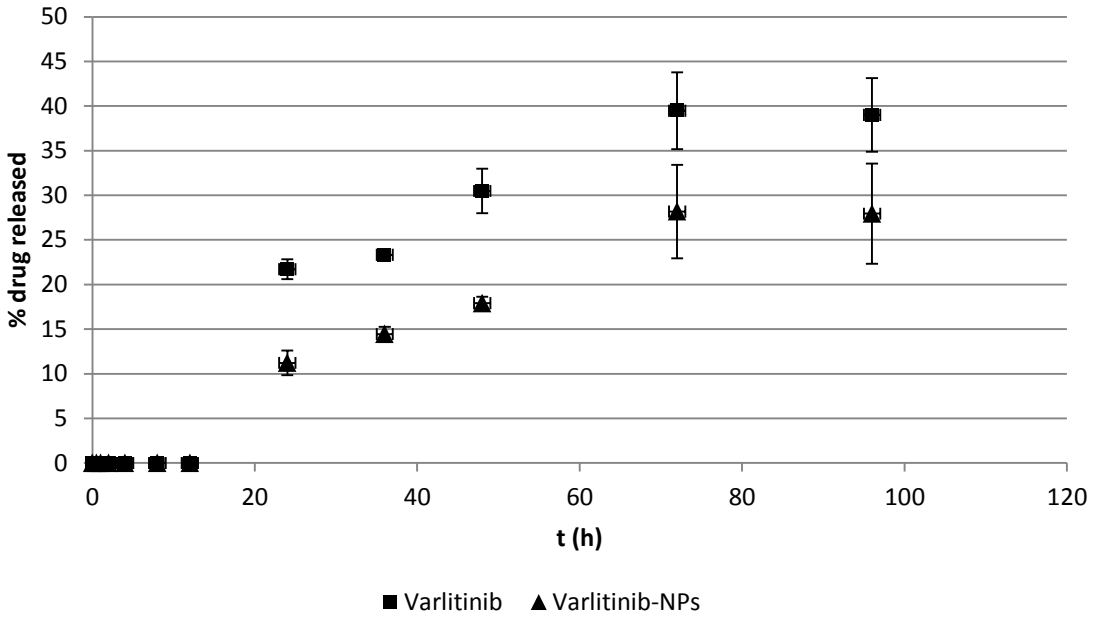

Figure 13-*In vitro* Release profile for Varlitinib conjugated PEG-AuNPs

Although the values for drug released cannot be determined prior to 24 hours, it is easily observable in Figure 13 a delay in the release of Varlitinib when conjugated with PEGAuNPs. At 24 hour the Varlitinib release is 22% and 11% for Varlitinib alone and conjugated with the PEGAuNPs, respectively. Therefore, it is clear that an interaction occurs between the drug and the nanoparticles, through covalent binding.

Conclusions and Future Perspectives

This thesis reports the design and characterization of nanocarriers – pegylated gold nanoparticles – conjugated with anticancer drugs to be used as drug delivery systems in cancer therapies.

According to the results obtained, a good pegylation of gold nanoparticles was achieved, increasing its stability in suspension for a long period of time. It was proved that particles are pH sensitive, which may be a surplus when regarding cellular studies.

It can also be shown that, for conjugation studies, both systems present good conjugation efficiency, especially for varlitinib, through covalent binding with the PEG chains at the nanoparticles surface. Additionally, *in vitro* release results show a controlled release of both antitumoral drugs when conjugated with the gold nanoparticles. These conjugated nanoparticles are also relatively stable for a short period of time at near-biological conditions, defining them as suitable for some assays regarding its cellular impact or therapeutic efficacy.

For future work, it is planned to access the stability of the nanoparticles in Fetal Bovine Serum (FBS), in order to mimic the biological environment. Moreover, cytotoxicity assays must be performed, to evaluate the toxicity of both PEGAuNPs and its respective conjugates towards cancer cell lines and normal cell lines. These assays will also allow the determination of the optimal concentration of nanoparticles at which they are biocompatible. Posteriorly, the internalization of the nanoparticles within the cells will be verified by laser scanning confocal microscopy. It is expected that the nanoparticles are localized in the cytoplasm with higher concentration in the perinuclear region, as observed in previous works of the group.

References

[1] D. M. Parkin, P. Pisani, and J. Ferlay, “Global cancer statistics,” *CA Cancer J Clin*, vol. 49, no. 2, pp. 1,33–64, 2011.

[2] J. D. Byrne, T. Betancourt, and L. Brannon-Peppas, “Active targeting schemes for nanoparticle systems in cancer therapeutics,” *Adv. Drug Deliv. Rev.*, vol. 60, no. 15, pp. 1615–1626, 2008.

[3] J. You, R. Zhang, C. Xiong, M. Zhong, M. Melancon, S. Gupta, A. M. Nick, A. K. Sood, and C. Li, “Effective photothermal chemotherapy using doxorubicin-loaded gold nanospheres that target EphB4 receptors in tumors,” *Cancer Res.*, vol. 72, no. 18, pp. 4777–4786, 2012.

[4] Y. J. Gu, J. Cheng, C. W. Y. Man, W. T. Wong, and S. H. Cheng, “Gold-doxorubicin nanoconjugates for overcoming multidrug resistance,” *Nanomedicine Nanotechnology, Biol. Med.*, vol. 8, no. 2, pp. 204–211, 2012.

[5] B. Asadishad, M. Vossoughi, and I. Alemzadeh, “Folate-receptor-targeted delivery of doxorubicin using polyethylene glycol-functionalized gold nanoparticles,” *Ind. Eng. Chem. Res.*, vol. 49, no. 4, pp. 1958–1963, 2010.

[6] E. Boisselier and D. Astruc, “Gold nanoparticles in nanomedicine: preparations, imaging, diagnostics, therapies and toxicity.,” *Chem. Soc. Rev.*, vol. 38, no. 6, pp. 1759–1782, 2009.

[7] S. Gill, R. Löbenberg, T. Ku, S. Azarmi, W. Roa, and E. J. Prenner, “Nanoparticles: Characteristics, Mechanisms of Action, and Toxicity in Pulmonary Drug Delivery—A Review,” *J. Biomed. Nanotechnol.*, vol. 3, no. 2, pp. 107–119, Jun. 2007.

[8] L. Dykman and N. Khlebtsov, “Gold nanoparticles in biomedical applications: recent advances and perspectives,” *Chem. Soc. Rev.*, vol. 41, no. 6, p. 2256, 2012.

[9] V. P. Torchilin, “Multifunctional nanocarriers.,” *Adv. Drug Deliv. Rev.*, vol. 58, no. 14, pp. 1532–55, Dec. 2006.

[10] M. C. Daniel and D. Astruc, “Gold Nanoparticles: Assembly, Supramolecular Chemistry, Quantum-Size-Related Properties, and Applications Toward Biology, Catalysis, and Nanotechnology,” *Chem. Rev.*, vol. 104, no. 1, pp. 293–346, 2004.

[11] W. Cai, T. Gao, H. Hong, and J. Sun, “Applications of gold nanoparticles in cancer nanotechnology.,” *Nanotechnol. Sci. Appl.*, vol. 2008, no. 1, pp. 17–32, 2008.

[12] R. Esfand and D. a. Tomalia, “Poly(amidoamine) (PAMAM) dendrimers: From biomimicry to drug delivery and biomedical applications,” *Drug Discov. Today*, vol. 6, no. 8, pp. 427–436, 2001.

[13] M. R. Papasani, G. Wang, and R. a. Hill, “Gold nanoparticles: The importance of physiological principles to devise strategies for targeted drug delivery,” *Nanomedicine Nanotechnology, Biol. Med.*, vol. 8, no. 6, pp. 804–814, 2012.

[14] W. H. De Jong and P. J. a Borm, “Drug delivery and nanoparticles:applications and hazards.,” *Int. J. Nanomedicine*, vol. 3, no. 2, pp. 133–149, 2008.

[15] P. Ghosh, G. Han, M. De, C. K. Kim, and V. M. Rotello, “Gold nanoparticles in delivery applications,” *Adv. Drug Deliv. Rev.*, vol. 60, no. 11, pp. 1307–1315, 2008.

[16] A. Kumari, S. K. Yadav, and S. C. Yadav, “Biodegradable polymeric nanoparticles based drug delivery systems,” *Colloids Surfaces B Biointerfaces*, vol. 75, no. 1, pp. 1–18, 2010.

[17] Z. Liu, Y. Jiao, Y. Wang, C. Zhou, and Z. Zhang, “Polysaccharides-based nanoparticles as drug delivery systems,” *Adv. Drug Deliv. Rev.*, vol. 60, no. 15, pp. 1650–1662, 2008.

[18] P. Ramos-Cabrer and F. Campos, “Liposomes and nanotechnology in drug development: focus on neurological targets.,” *Int. J. Nanomedicine*, vol. 8, pp. 951–60, Jan. 2013.

[19] S. Vemuri and C. T. Rhodes, “Preparation and characterization of liposomes as therapeutic delivery systems: A review,” *Pharm. Acta Helv.*, vol. 70, no. 2, pp. 95–111, 1995.

[20] B. Maherani, E. Arab-Tehrany, M. R. Mozafari, C. Gaiani, and M. Linder, “Liposomes: A Review of Manufacturing Techniques and Targeting Strategies,” *Curr. Nanosci.*, vol. 7, no. 3, pp. 436–452, 2011.

[21] S. Aryal, J. J. Grailer, S. Pilla, D. a. Steeber, and S. Gong, “Doxorubicin conjugated gold nanoparticles as water-soluble and pH-responsive anticancer drug nanocarriers,” *J. Mater. Chem.*, vol. 19, no. 42, p. 7879, 2009.

[22] I. Brigger, C. Dubernet, and P. Couvreur, “Nanoparticles in cancer therapy and diagnosis,” *Adv. Drug Deliv. Rev.*, vol. 54, no. 5, pp. 631–651, 2002.

[23] M. R. Mozafari, C. Johnson, S. Hatziantoniou, and C. Demetzos, “Nanoliposomes and their applications in food nanotechnology.,” *J. Liposome Res.*, vol. 18, no. 4, pp. 309–27, Jan. 2008.

[24] N. Ribeiro, S. R. Sousa, C. a van Blitterswijk, L. Moroni, and F. J. Monteiro, “A biocomposite of collagen nanofibers and nanohydroxyapatite for bone regeneration.,” *Biofabrication*, vol. 6, no. 3, p. 035015, Jun. 2014.

[25] H. Maeda, G. Y. Bharate, and J. Daruwalla, “Polymeric drugs for efficient tumor-targeted drug delivery based on EPR-effect,” *Eur. J. Pharm. Biopharm.*, vol. 71, no. 3, pp. 409–419, 2009.

[26] J. Fang, H. Nakamura, and H. Maeda, “The EPR effect : Unique features of tumor blood vessels for drug delivery , factors involved , and limitations and augmentation of the effect,” *Adv. Drug Deliv. Rev.*, vol. 63, no. 3, pp. 136–151, 2011.

[27] D. Xiaowei and J. M. Russell, “Nanomedicinal strategies to treat multidrug-resistant tumors: Current Progress,” *Nanomedicine*, vol. 5, no. 4, pp. 597–615, 2011.

[28] S. K. Seol, D. Kim, S. Jung, W. S. Chang, and J. T. Kim, “One-step synthesis of PEG-coated gold nanoparticles by rapid microwave heating,” *J. Nanomater.*, vol. 2013, 2013.

[29] J. Kimling, M. Maier, V. Okenve, V. Kotaidis, H. Ballot, a Plech, and B. Okenve, “Turkevitch method for gold nanoparticle synthesis revisited,” *J. Phys. Chem. B*, vol. 110, no. 95 mL, pp. 15700–15707, 2006.

[30] M. Brust, M. Walker, D. Bethell, D. J. Schiffrin, and R. Whyman, “Synthesis of Thiol-derivatised Gold Nanoparticles in,” *J. Chem. Soc.*, pp. 801–802, 2000.

[31] S. S. Agasti, S. Rana, M. H. Park, C. K. Kim, C. C. You, and V. M. Rotello, “Nanoparticles for detection and diagnosis,” *Adv. Drug Deliv. Rev.*, vol. 62, no. 3, pp. 316–328, 2010.

[32] S. A. Kumar, S. A. Kumar, Y.-A. Peter, Y.-A. Peter, J. L. Nadeau, and J. L. Nadeau, “Facile biosynthesis, separation and conjugation of gold nanoparticles to doxorubicin,” *Nanotechnology*, vol. 19, no. 49, p. 495101, 2008.

[33] J. Gao, X. Huang, H. Liu, F. Zan, and J. Ren, “Colloidal stability of gold nanoparticles modified with thiol compounds: bioconjugation and application in cancer cell imaging.,” *Langmuir*, vol. 28, no. 9, pp. 4464–71, 2012.

[34] R. Bhattacharya, C. R. Patra, R. Verma, S. Kumar, P. R. Greipp, and P. Mukherjee, “Gold Nanoparticles Inhibit the Proliferation of Multiple Myeloma Cells,” *Adv. Mater.*, vol. 19, no. 5, pp. 711–716, 2007.

[35] S. C. Coelho, G. Almeida, M. C. Pereira, F. Santos-Silva, M. A.N., and Coelho, “Functionalized Gold Nanoparticles improve Afatinib delivery into Cancer cells,” 2012.

[36] S. C. Coelho, S. Rocha, M. C. Pereira, P. Juzenas, and M. A. N. Coelho, “Enhancing Proteasome-Inhibitor Effect by Functionalized Gold Nanoparticles,” *J. Biomed. Nanotechnol.*, vol. 9, no. xx, pp. 1–7, 2013.

[37] H. G. Keizer, H. M. Pinedo, G. J. Schuurhuis, and H. Joenje, “Doxorubicin (adriamycin): a critical review of free radical-dependent mechanisms of cytotoxicity.,” *Pharmacol. Ther.*, vol. 47, no. 2, pp. 219–231, 1990.

[38] S. Chalasani, K. V. Prakash, R. P. Pulla, R. Tekula, and B. Umasankar, “Development and Validation of Doxorubicin Hcl in Spectrophotometry,” vol. 3, no. 3, pp. 216–218, 2013.

[39] S. Granados-Principal, J. L. Quiles, C. L. Ramirez-Tortosa, P. Sanchez-Rovira, and Mc. Ramirez-Tortosa, “New advances in molecular mechanisms and the prevention of adriamycin toxicity by antioxidant nutrients,” *Food Chem. Toxicol.*, vol. 48, no. 6, pp. 1425–1438, 2010.

[40] A. de Luca, N. Moroni, A. Serafino, A. Primavera, A. Pastore, J. Z. Pedersen, R. Petruzzelli, M. G. Farrace, P. Pierimarchi, G. Moroni, G. Federici, P. Sinibaldi Vallebona, and M. Lo Bello, “Treatment of doxorubicin-resistant MCF7/Dx cells with

nitric oxide causes histone glutathionylation and reversal of drug resistance," *Biochem. J.*, vol. 440, no. 2, pp. 175–183, 2011.

[41] M. Zimmermann, A. S. Arachchige-Don, M. S. Donaldson, R. F. Dallapiazza, C. E. Cowan, and M. C. Horne, "Elevated cyclin G2 expression intersects with DNA damage checkpoint signaling and is required for a potent G2/M checkpoint arrest response to doxorubicin," *J. Biol. Chem.*, vol. 287, no. 27, pp. 22838–22853, 2012.

[42] G. Mandili, A. Khadjavi, V. Gallo, V. G. Minero, L. Bessone, F. Carta, G. Giribaldi, and F. Turrini, "Characterization of the protein ubiquitination response induced by Doxorubicin," *FEBS J.*, vol. 279, no. 12, pp. 2182–2191, 2012.

[43] W. Sun, A. L. Kalen, B. J. Smith, J. J. Cullen, and L. W. Oberley, "Enhancing the antitumor activity of adriamycin and ionizing radiation," *Cancer Res.*, vol. 69, no. 10, pp. 4294–4300, 2009.

[44] J. Spadavecchia, R. Perumal, A. Barras, J. Lyskawa, P. Woisel, W. Laure, C.-M. Pradier, R. Boukherroub, and S. Szunerits, "Amplified plasmonic detection of DNA hybridization using doxorubicin-capped gold particles.," *Analyst*, vol. 139, no. 1, pp. 157–164, 2014.

[45] N. S. Elbialy, M. M. Fathy, and W. M. Khalil, "Doxorubicin loaded magnetic gold nanoparticles for in vivo targeted drug delivery," *Int. J. Pharm.*, vol. 490, no. 1–2, pp. 190–199, 2015.

[46] J. T. Hartmann, M. Haap, H.-G. Kopp, and H.-P. Lipp, "Tyrosine kinase inhibitors - a review on pharmacology, metabolism and side effects.," *Curr. Drug Metab.*, vol. 10, no. 5, pp. 470–481, 2009.

[47] A. Arora and E. Scholar, "Role of tyrosine kinase inhibitors in cancer therapy," *J. Pharmacol. Exp. …*, vol. 315, no. 3, pp. 971–979, 2005.

[48] E. Mini, S. Nobili, B. Caciagli, I. Landini, and T. Mazzei, "Cellular pharmacology of gemcitabine," *Ann. Oncol.*, vol. 17, no. SUPPL. 5, pp. 7–12, 2006.

[49] H. W. Kao, Y. Y. Lin, C. C. Chen, K. H. Chi, D. C. Tien, C. C. Hsia, M. H. Lin, and H. E. Wang, "Evaluation of EGFR-targeted radioimmuno-gold-nanoparticles as a theranostic agent in a tumor animal model," *Bioorganic Med. Chem. Lett.*, vol. 23, no. 11, pp. 3180–3185, 2013.

[50] G. Miknis, "ARRY-334543, a Potent, Orally Active, Small Molecule Inhibitor of EGFR and ErbB-2," *Array BioPharma Inc.*, 2007.

[51] P. Baptista, G. Doria, D. Henriques, E. Pereira, and R. Franco, "Colorimetric detection of eukaryotic gene expression with DNA-derivatized gold nanoparticles," *J. Biotechnol.*, vol. 119, no. 2, pp. 111–117, 2005.

[52] J. Holoubek, "Some applications of light scattering in materials science," *J. Quant. Spectrosc. Radiat. Transf.*, vol. 106, no. 1–3, pp. 104–21, 1995.

[53] W. I. I. Goldburg, "Dynamic light scattering," *Am. J. Phys.*, vol. 67, no. 12, pp. 1152–1160, 1999.

[54] J. M. Freire, M. M. Domingues, J. Matos, M. N. Melo, A. S. Veiga, N. C. Santos, and M. a R. B. Castanho, "Using zeta-potential measurements to quantify peptide partition to lipid membranes," *Eur. Biophys. J.*, vol. 40, no. 4, pp. 481–487, 2011.

[55] M. Kaszuba, J. Corbett, F. M. Watson, and A. Jones, “High-concentration zeta potential measurements using light-scattering techniques.,” *Philos. Trans. A. Math. Phys. Eng. Sci.*, vol. 368, no. 1927, pp. 4439–4451, 2010.

[56] H. Silva, *Espectroscopia no infravermelho por transformada de Fourier (FTIR). Fundamentos e aplicação na caracterização de materiais de construção*. Lisbon: LNEC, 2007.

[57] P. R. Griffiths, *Fourier Transform Infrared Spectrometry*. Wiley-Interscience, 2007.

[58] J. R. Lakowicz, “Principles of Fluorescence Spectroscopy,” *Princ. Fluoresc. Spectrosc.*, pp. 1–23, 2006.

[59] X. Dai, Z. Yue, M. E. Eccleston, J. Swartling, N. K. H. Slater, and C. F. Kaminski, “Fluorescence intensity and lifetime imaging of free and micellar-encapsulated doxorubicin in living cells,” *Nanomedicine Nanotechnology, Biol. Med.*, vol. 4, no. 1, pp. 49–56, 2008.

[60] L. Reimer and H. Kohl, *Transmission Electron Microscopy*. NY, USA, 2008.

[61] D. B. Williams and C. B. Carter, “Transmission electron microscopy: A textbook for materials science,” *Transm. Electron Microsc. A Textb. Mater. Sci.*, no. September 2015, pp. 1–760, 2009.

[62] R. H. . Haschemeyer, “Negative Staining,” *Princ. Tech. Electron Microsc. - Biol. Appl.*, 1972.

[63] G. C. Baltazar, S. Guha, W. Lu, J. Lim, K. Boesze-Battaglia, A. M. Laties, P. Tyagi, U. B. Kompella, and C. H. Mitchell, “Acidic Nanoparticles Are Trafficked to Lysosomes and Restore an Acidic Lysosomal pH and Degradative Function to Compromised ARPE-19 Cells,” *PLoS One*, vol. 7, no. 12, pp. 1–10, 2012.

[64] S. Rana, a. Gallo, R. S. Srivastava, and R. D. K. Misra, “On the suitability of nanocrystalline ferrites as a magnetic carrier for drug delivery: Functionalization, conjugation and drug release kinetics,” *Acta Biomater.*, vol. 3, no. 2, pp. 233–242, 2007.

[65] A. Z. Mirza and H. Shamshad, “Preparation and characterization of doxorubicin functionalized gold nanoparticles,” *Eur. J. Med. Chem.*, vol. 46, no. 5, pp. 1857–1860, May 2011.

[66] W. Gallagher, “Infrared Spectroscopy : Theory,” *J. Mol. Spectrosc.*, vol. 214, no. 1, pp. 155–164, 2002.

[67] S. Pine, *Organic Chemistry*. 1987.

[68] S. C. Coelho, S. Rocha, P. Juzenas, P. Sampaio, G. M. Almeida, F. S. Silva, M. C. Pereira, and M. a N. Coelho, “Gold nanoparticle delivery-enhanced proteasome inhibitor effect in adenocarcinoma cells.,” *Expert Opin. Drug Deliv.*, pp. 1–8, 2013.

[69] S. C. Coelho, S. Rocha, P. Sampaio, M. C. Pereira, and M. a. N. Coelho, “Encapsulation of a proteasome inhibitor with gold-polysaccharide nanocarriers,” *J. Nanoparticle Res.*, vol. 16, no. 4, p. 2368, 2014.